Available online at www.sciencedirect.com
ScienceDirect
Earth and Planetary Science Letters 250 (2006) 214–223
EPSL
www.elsevier.com/locate/epsl

Automatic detection and rapid determination of earthquake magnitude by wavelet multiscale analysis of the primary arrival

Frederik J. Simons [a,*], Ben D. E. Dando [a,1], Richard M. Allen [b]

[a] University College London, Department of Earth Science, Gower Street, London WC1E 6BT, United Kingdom
[b] Department of Earth and Planetary Science, University of California, Berkeley CA 94720, United States

Received 17 May 2006; received in revised form 20 July 2006; accepted 24 July 2006
Available online 1 September 2006
Editor: R.D. van der Hilst

Abstract

Earthquake early warning systems must save lives. It is of great importance that networked systems of seismometers be equipped with reliable tools to make rapid determinations of earthquake magnitude in the few to tens of seconds before the damaging ground motion occurs. A new fully automated algorithm based on the discrete wavelet transform detects as well as analyzes the incoming first arrival with great accuracy and precision, estimating the final magnitude to within a single unit from the first few seconds of the *P* wave.

Keywords: Wavelets; Time–frequency analysis; Earthquake magnitude determination; *P* wave amplitude

1. Introduction

Determining earthquake magnitudes quickly is of great utility in disaster prevention. Even within the short time span of a few seconds, a well-calibrated automated alarm system can be triggered, for instance, to halt trains, turn off power stations and broadcast alarms to the general population, thereby avoiding physical and personal damage [1]. As the cost of raising false alarms is significant, such alarm systems have to be carefully configured. Earthquake early-warning systems must also be simple in design, so that relatively low-technology systems, perhaps even battery-operated ones, can be easily equipped with the processing technology required.

Several seconds elapse between the arrival of the first *P* wave at the monitoring station and the arrival of the damaging *S* and surface waves, and this time interval increases when the recording stations are located in an area close to the likely earthquake sources yet at some distance away from densely populated areas. Recent systems deployed in California and Japan have relied on sequential algorithms to measure the dominant period in the *P* wave arrival as an observable broadly diagnostic of the earthquake magnitude [2–4].

Such systems are more or less empirical. While research has been done on the spectrum of seismic waves

* Corresponding author.
E-mail address: fjsimons@alum.mit.edu (F.J. Simons).
URL: www.frederik.net (F.J. Simons).
[1] Now at: University of Leeds, School of Earth and Environment, Leeds LS2 9JT, United Kingdom.

0012-821X/$ - see front matter © 2006 Elsevier B.V. All rights reserved.
doi:10.1016/j.epsl.2006.07.039

emitted by sources of various sizes [5–7], the nature of wave propagation (which includes the effects on the *P* wave amplitude due to focusing, attenuation and site amplification) as well as the complexities of the source mechanism, and its orientation with respect to the measurement stations, are all such that any predictive relationships between the observables gleaned from the *P* wave and earthquake magnitude are statistical at best.

In this paper we present a fully automated algorithm that dramatically improves the reliability of magnitude determination from the first few seconds of the waveform, with a speed and simplicity far exceeding previous attempts. Our algorithm has not been designed to suit a particular station configuration, or size or distribution of events. We use the database of 53 southern Californian events identical to that used by Allen and coworkers [2,8], and apply the procedure to 2272 seismograms recorded at stations of the TriNet array (see Fig. 1), at distances from the source of up to 150 km. We window the seismograms to within 4 s from the iasp91 predicted *P* arrival time [9]. Other than that, our approach is entirely agnostic of seismology, and it has no tunable parameters.

2. Time–frequency analysis

Two example waveforms are shown in Fig. 2. The sampling rate is 20 Hz. As Kanamori [1] put it, the *S* wave carries energy; the *P* wave carries information: until now, seismologists have commonly sought a correlation between the earthquake magnitude and the predominant period of the *P* wave. This observable is τ_c, where

$$\tau_c^2 = 4\pi^2 \frac{\int_0^{\tau_0} u^2(t)\mathrm{d}t}{\int_0^{\tau_0} \dot{u}^2(t)\mathrm{d}t} = \frac{\int_0^{\infty} |\hat{u}(f)|^2 \mathrm{d}f}{\int_0^{\infty} f^2 |\hat{u}(f)|^2 \mathrm{d}f}. \quad (1)$$

Here, $u(t)$ and $\dot{u}(t)$ are the ground motion displacement and velocity as a function of time t, respectively, and τ_0 is the duration of the *P* waveform. This is usually taken to be 3 or 4 s, and τ_c is determined using an iterative algorithm that can be used in real-time [2].

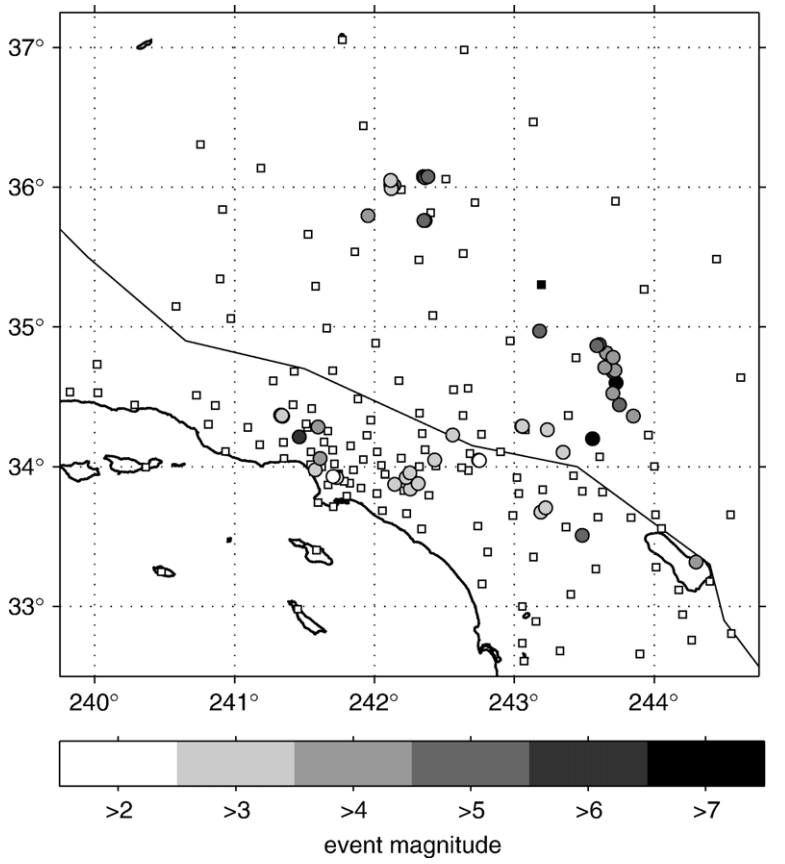

Fig. 1. Map of southern California showing the locations of 142 TriNet stations (squares) and epicenters of 53 earthquakes used in this study (circles). The solid black square is Goldstone (GSC).

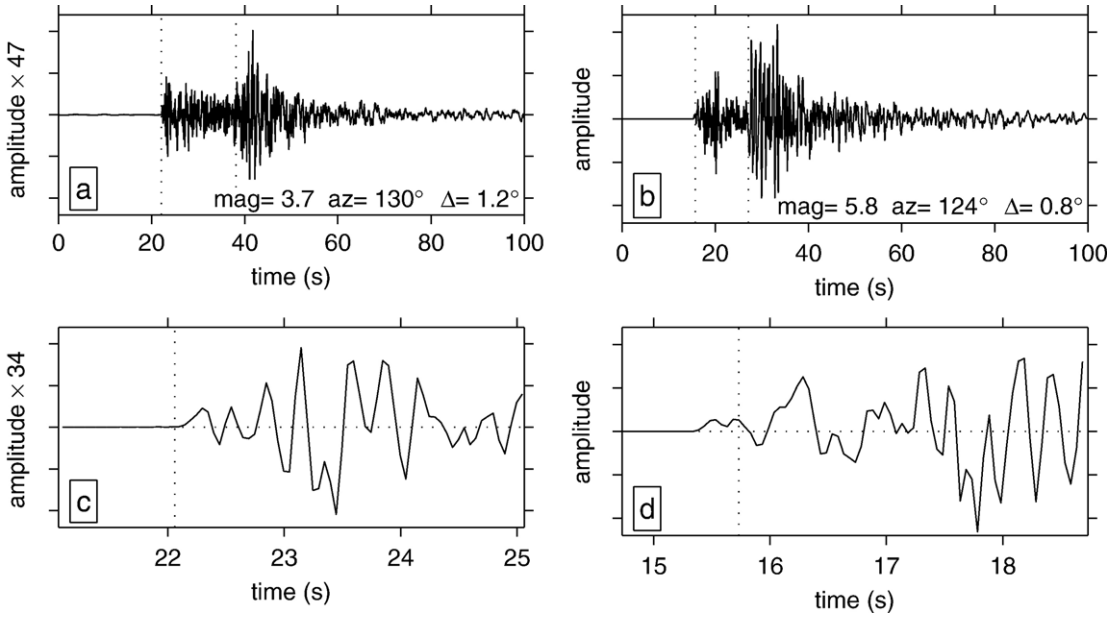

Fig. 2. Waveforms recorded by station GSC (Goldstone, California; location marked in Fig. 1). The top panels show vertical-component seismograms of (a) a magnitude 3.7 event at 2.8 km depth on July 30th 2001 and (b) a magnitude 5.8 event at 5.4 km depth on September 20th 1995. Magnitude (mag), azimuth (az) and epicentral distance (Δ) are shown inside the top panels. The theoretical arrival times of the *P* and *S* waves in the iasp91 reference Earth model are marked by the dotted vertical lines. The bottom panels (c) and (d) show zooms of the first arriving *P* wave, windowed −1 and +3 s about the predicted arrival time. The vertical scales of the smaller event have been amplified by the factor indicated on the axes. Sampling rate is 20 Hz.

The time-domain expression (the left-hand side of Eq. (1)) reveals that calculating τ_c is plagued by instability: the ratio of the energy of a signal to the energy in its first derivative is notoriously hard to compute [10]. Moreover, the spectral-domain expression (the right-hand side of Eq. (1)) shows that τ_c is a weighted measure of the spectral energy density in the signal, derived from its Fourier transform $\hat{u}(f)$ as a function of frequency f. It thus blurs the information contained in the time-frequency representation of the signal. Finally, this representation itself, obtained computationally from the Fourier transform of (windowed and overlapping segments of) the data, is a redundant transformation of the one-dimensional sampled time series to a regularly sampled two-dimensional time-frequency plane [11,12]. In other words, this, too, is an inefficient and unstable approach to computing the predominant period.

The time-frequency properties of the seismograms shown in Fig. 2 are illustrated by the spectrograms in Fig. 3. The spectrograms, showing the time-dependent spectral density of the waveforms (resampled at 10 Hz), were computed using a Welch overlapping segment algorithm using a Hann taper and 50% window overlap [13]. Superimposed is $1/\tau_c$ (the thick black curve) as resulting from the left-hand side of Eq. (1), using a one-sided first difference to approximate the derivative and maintaining $\tau_0=4$ s. The computation of τ_c was carried out on (unwindowed) segments at locations identical to those used to calculate the spectrograms; values are displayed at the midpoints of the overlapping data sections. The predominant frequency, as defined by Eq. (1), meanders through the spectral density. It reaches finite non-zero values even before the onset of the *P* wave, even though, as can be seen from Fig. 2, the signal there is non-existent and essentially noise-free. These drawbacks are responsible for the high scatter and limited predictive capability of the predominant frequency in previous work [2–4,7].

3. Wavelet analysis

The shortcomings of spectrogram analysis and the difficulties in stably estimating the predominant frequency of a seismogram are entirely removed by switching from the time-frequency to the time-scale domain. Originally introduced for applications to seismology [14,15], wavelet analysis has attracted a cult following mostly among engineers and applied mathematicians — even, it appears, among English majors [16]. The wavelet literature is vast but accessible accounts of the main ideas are given in

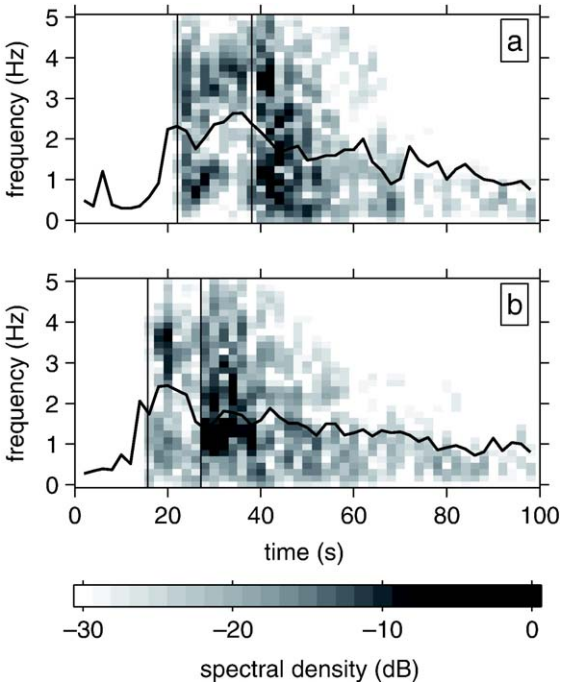

Fig. 3. Time-frequency analysis of waveforms (a) and (b) of Fig. 2 (resampled at 10 Hz). Shown is the logarithmic amplitude of the spectral density (in units of energy per frequency) on a decibel scale, calculated (in 64 frequency bins) over 4 s sliding segments of the data, overlapping by 50% and windowed with a Hann taper. The thin solid vertical lines mark the iasp91 arrival times of the *P* and the *S* waves. The thick black curve is the predominant frequency measured over the same 4 s intervals by the method described in the text.

various works intended for those familiar with signal processing [17], computer graphics [18] and filter banks [19], or for geophysicists [20]. Here we show that the absolute magnitude of the wavelet coefficients coding for the *P* wave arrival at a particular scale is related to the earthquake magnitude in a diagnostic manner vastly more useful than the time-frequency measure that we discussed in the previous section.

The central feature of the discrete wavelet transform pertaining to this study is its non-redundant nature: rather than estimating the amplitudes belonging to certain frequencies at certain times, as was done to construct the spectrograms of Fig. 3, the discrete wavelet transform finds the time-dependent contributions to the waveform in terms of coarseness or scale. It does this on a dyadic grid: the time-scale plane is tiled such that coarse scales are sampled in the time-domain at half the rate of the next finer scale. As a result, the wavelet transform generates exactly as many scale-dependent coefficients as there are samples in the seismogram, without requiring redundant computations detrimental to the speed of an early-warning system.

There are numerous possible wavelet bases [11,12] and computational algorithms [21,22]. We use a biorthogonal construction [23] with two and four vanishing moments for the primal and dual wavelets, respectively, and abbreviate this as the CDF (2,4) construction. The wavelet and scaling basis functions are short and not entirely dissimilar to the zooms on the *P* wave shown in Fig. 2. As with any basis expansion, fewer coefficients are needed as the shape of the basis better approximates the signal at the outset.

We use the fast algorithm known as the lifting approach, due to Sweldens [24]. Besides boasting a computation speed that is asymptotically (as the number of vanishing moments increases) twice as fast as the polyphase algorithm [21,22,25], the lifting scheme has two additional advantages. Firstly, the coefficients can be computed in-place without allocating extra memory, and secondly, intermediate operations can be rounded to allow for integer-to-integer transformations [26]. These properties may well be mission-critical in a variety of real-world contexts where small fixed buffers record limited-precision data and computation is performed on very low-power chips [27].

The algorithms for the forward as well as the inverse CDF (2,4) transforms, over five scales, are of an intuitively as well as practically very appealing simplicity (see the Appendix). The signal is subjected to a few iterations of an algorithm that halves the number of samples processed at every step, effectively rearranging the time-domain samples to coefficients ordered on a scale from fine to coarse.

Arranged in the so-called Mallat multi-resolution ordering, the result of the wavelet transform of an input data vector x of length N, where N is a power of two, is contained in the same-length vector x, where the coarsest-scale scaling coefficients, at the fifth scale, comprise the first $N/(2\hat{}5)$ entries. These represent the least detailed level of approximation into which the signal is broken down. They are followed by the wavelet coefficients, which contain the details missing from the scaling coefficients at decreasing levels of coarseness, at the scales 5, 4, 3, 2 and 1. Those are grouped in vectors of length $N/(2\hat{}5)$, $N/(2\hat{}4)$, $N/(2\hat{}3)$, $N/(2\hat{}2)$, and $N/(2\hat{}1)$; the total signal length is preserved. The magnitude of the scaling and wavelet coefficients contains the amplitude information that is effectively discarded by algorithms that exclusively recover the predominant period and thereby reduce the signal to a single number. The lifting algorithm does not require the signal to have a number of samples that is a power of two, but in the shorthand notation in which it is presented in the Appendix, this is simply more convenient.

The time-scale deconstruction of the same waveforms plotted in Fig. 2 (resampled at 10 Hz) is shown in Fig. 4. The magnitudes of the wavelet coefficients are shown. The dyadic nature of the time-scale tiling is clearly visible as blocks of constant value whose length increases with increasing scale or coarseness. The color scale is linear, and identical for both waveforms: the energies from the *P* and the *S* arrivals are clearly distinguished.

4. Multiscale amplitudes and local magnitude

To translate a wavelet-transformed seismogram (sampled at 20 Hz) to a measurement containing information about the magnitude of the earthquake source we propose the following. The CDF (2,4) decomposition yields wavelet coefficients calculated over a total of five scales. We study the correlation of their averages over all stations, $C_1 \rightarrow C_5$, to the earthquake magnitude, and derive best-fit regression lines from which the magnitude of new observations may be predicted. We maintain an upper limit of coarseness at scale 5; the effective support of the wavelet basis function at that scale corresponds to about 3.2 s of the 20 Hz signal. Although real-time applications may be slightly affected by the presence of the boundary (i.e. of a finite-length signal known only up the end point [12,22]), in practice, this means that a magnitude determination is available within 3–4 s after the initial onset of the *P* wave.

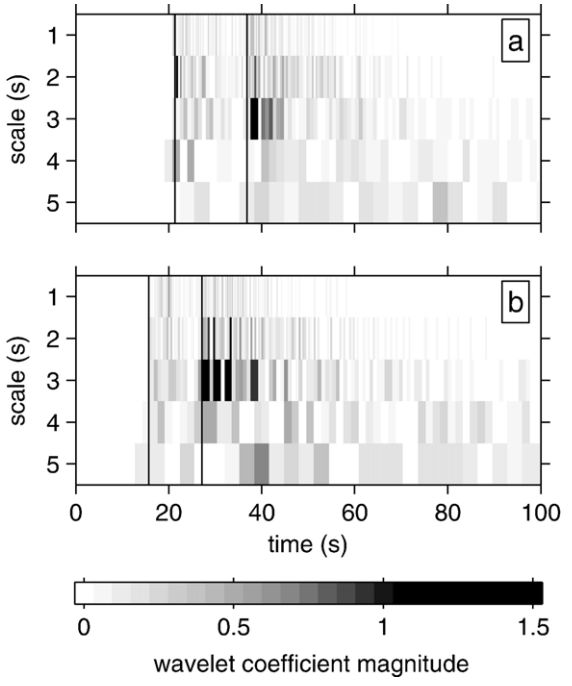

Fig. 4. Time-scale analysis of the waveforms (a) and (b) of Fig. 2 (resampled at 10 Hz). The absolute magnitudes of the unthresholded wavelet coefficients calculated in the biorthogonal Cohen–Daubechies–Feauveau (2,4) basis are shown on a common linear color scale. The thin solid vertical lines mark the iasp91 arrival times of the *P* and the *S* waves. Scale is a loose measure of frequency; higher scale numbers represent lower-frequency, or coarser, information. The energies from the *P* and the *S* arrivals are clearly visible and distinct.

This length of time represents an acceptable compromise between speed and accuracy of the magnitude prediction (which, as we shall see, is excellent), and is the appropriate interval for a comparison of the new method with traditional time-frequency methods, which usually use a 4 s time window to provide stability to the determination of the predominant period [2,4]. The curious observation that such brief segments of the seismogram may contain information about the final magnitude even of very large earthquakes, which occur on faults that may rupture over tens of seconds, is central to a debate in the seismological community [7,28,29] which we hope to stimulate but cannot attempt to address within the scope of this paper.

Our data set consists of sections of seismograms windowed ±4 s about the predicted *P* arrival time in the iasp91 Earth model. In practice, as can be seen in Fig. 2, the actual arrival of the *P* wave is slightly offset from this reference value. Indeed, our algorithm must not know when the *P* wave is about to come in: rather, it must be capable of detecting as well as diagnosing the incoming first break, even if the seismogram is noisy.

This is achieved by wavelet shrinkage, where low-magnitude, statistically insignificant, wavelet coefficients are reduced to zero following a scale-dependent thresholding scheme [30]. The first significant coefficient at every scale contains information about the *P* wave, and its averages over all stations will be used to derive the best-fitting trends. In practice, the threshold T_j at scale j is defined in terms of a spread estimate $\hat{\sigma}_j$ and the number of coefficients at that scale N_j, as

$$T_j = \hat{\sigma}\sqrt{2\ln N_j}, \tag{2}$$

whereby $\hat{\sigma}$ is the median absolute deviation from the median of the coefficients, divided by 0.6745 (the expectation of the median absolute deviation of standard normally distributed coefficients) [31]. Soft thresholding, then, is achieved by replacing the original coefficients by their signed distance from the threshold, thus decreasing by T the amplitude of all coefficients that are above T [12]. The zeroing of insignificant wavelet coefficients results in a denoised, compressed representation of the signal. We take the first nonzero thresholded coefficient at every scale to be our primary observable and analyze it as such.

The results of our analysis are shown in Fig. 5. For every one of the 2272 seismograms recorded at the 142 stations, at source distances of up to 150 km, we plot the first significant wavelet coefficients at scales 2 through 5 in function of the TriNet magnitude of the 53 identified events (noting that some share the same magnitude, which improves the statistics: 34 distinct magnitudes were observed on a minimum of 2 and a maximum of 113 seismic traces). Out of the total number of records, six *P* waves of small earthquakes remained undetected in that they failed to turn up as significant wavelet coefficients at any scale.

The percentage of the recordings with significant wavelet coefficients in the 8 s analysis window is shown in the legend. This percentage falls predictably across the scales. Within a certain scale (not shown) the detected percentage for individual magnitudes increases with the magnitude, and the smaller events are less likely to show up in the larger scales. These statistics may serve as an evaluation of our detection algorithm: of the 2272 traces containing events, 99.74% were detected at one or more scales, and the scale up to which they were observed increases proportionally to the event magnitude.

The thresholded wavelet amplitudes at scales 2 to 5 are plotted versus TriNet magnitude in Fig. 5 (gray dots). Averages over every one of 34 distinct magnitudes are shown by the black dots. An idea of the width of their distribution can be obtained from their 25th and 75th percentiles, shown as short horizontal dashes. We divide the TriNet magnitude into a low ($m_l \leq 5.02$) and high ($m_h > 5.02$) magnitude range [2], and compute correlation coefficients between wavelet amplitude and earthquake magnitude in both ranges, R_l and R_h. These

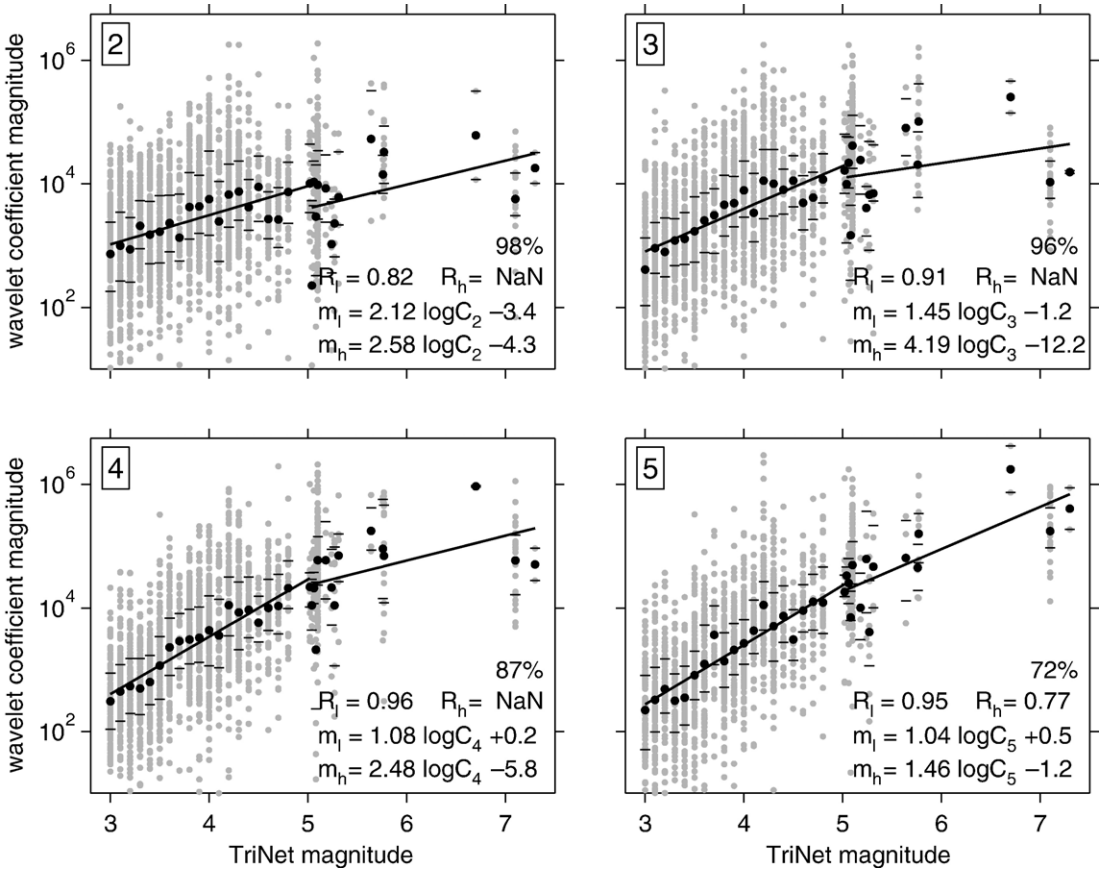

Fig. 5. The correlation of wavelet-scale dependent amplitudes with earthquake magnitude. The panels numbered 2 through 5 show the absolute magnitude of the first significant (after thresholding as described in the text, and with the percentage of incoming *P* waves detected at each scale marked in the lower right corner) wavelet coefficients in the Cohen–Daubechies–Feauveau (2,4) basis, at scales 2 through 5, on a logarithmic scale, automatically determined from 8 s of data symmetrically windowed around the iasp91 *P* arrival time. Results for individual seismograms are shown as gray dots, the 25th and 75th percentile by the thin black dashes, and the averages, $C_2 \rightarrow C_5$, at every distinct event magnitude by the black dots. The superimposed thick black lines are least-squares best-fit lines to the average values over a low (m_l) and high (m_h) magnitude range, parameterized by the equations listed in the lower right. The correlation coefficients R_l and R_h are quoted only where they exceed the 95% significance level.

are stated in the legend only when they exceed the 95% confidence level (based on an assumed normal distribution; we write NaN elsewhere). Regression lines are determined from least-squares fitting to give a relation between the average of the thresholded coefficients at a particular scale, $C_2 \rightarrow C_5$, and the local TriNet earthquake magnitude.

The scatter about the best-fitting trends is smaller than that observed using the predominant period as an observable [2,4]. Furthermore, while the results in earlier studies were limited to recordings located up to 100 km away from the source, ours included all those up to 150 km. Abandoning the time-frequency approach and switching completely to a wavelet-based method greatly improves and enhances the applicability of our method.

5. Discussion: Accurate magnitude prediction

As shown in Fig. 5, significant correlations exist between the station-averaged thresholded wavelet coefficients and the low-range event magnitude m_l at all scales, whereas the only significant correlation between the high magnitudes m_h and the wavelet observable is at scale 5. This scale holds the most promise in making quick event magnitude determinations directly from the seismogram (even if the smaller scales are more useful in providing the basic detection capability). Since the coefficients at all scales $j \leq 5$ are known when the computation is carried out to this largest scale (see the Appendix), any or all of the linear regression lines may be used to provide an estimate of the event magnitude from the station-averaged coefficients.

The error with which the magnitude can be predicted varies across the scales, as can be observed in Fig. 5. The differences between the true magnitude and that predicted from either regression relation range from −2.3 to +3.3 at scale 2, −3.8 to +4.0 at scale 3, −2.3 to +2.7 at scale 4 and −1.2 to +1.2 at scale 5, where a negative value indicates an earthquake whose magnitude has been overpredicted. These numbers are virtually unchanged when the appropriate regression line is used: −2.3 to +3.5 at scale 2, −3.8 to +4.2 at scale 3, −2.3 to +2.7 at scale 4 and −1.2 to +1.2 at scale 5. In other words, prediction at a given scale with either regression line leads to an unacceptable range of magnitudes, except at scale 5.

Only between scales 2 and 5 are the prediction errors completely uncorrelated at the 95% confidence level (not shown). However, the errors obtained by averaging the predictions from scales 2 and 5 are larger than those obtained from scale 5 alone. The excellent predictive capability of the thresholded wavelet coefficients from scale 5 only is illustrated for all 53 events in Fig. 6a. Using the average of the magnitudes predicted from both regression lines (shown by the black circles) results in a prediction error that ranges from −0.7 to 1.2, where the asymmetry indicates the conservative tendency to underrather than overpredict.

Fig. 6b shows the number of stations that were available to make the magnitude predictions for all 53 events of Fig. 6a. The numbers range from a minimum of 2 to a maximum of 64 traces. The relative dearth of observations in the high-magnitude range is all the more unfortunate since directivity is expected to affect the reliability of the determination for the largest events. However, Fig. 6c demonstrates that the number of reporting stations does not have an influence on the predictive capacity of our method, as measured by the absolute misfit of the estimated versus the true magnitudes. Without additional observations and a more detailed treatment of the influence of the earthquake radiation pattern and the azimuthal distribution of the recording stations, both of which are outside the scope of this paper, we interpret this as much as empirical evidence of the promise of our method as encouragement for further study.

To summarize: based on 2272 traces of 53 events with 34 distinct magnitudes, we advocate performing a CDF (2,4) discrete wavelet transform down to the fifth scale of coarseness (by the forward algorithm in the Appendix) on all traces of a given seismic array. As long as the incoming records consist merely of random noise, the wavelet coefficients are unlikely to be significant and exceed the thresholds defined in Eq. (2), but if any or all of them do, an event may be considered detected. An average is formed over all detecting stations of the absolute value of the first significant wavelet coefficient at the fifth scale: this quantity, C_5, is diagnostic of the event magnitude. With hindsight, this number predicts an earthquake magnitude, m, from the relation

$$m_l = 1.04\ \log C_5 + 0.5 \tag{3}$$

if the true magnitude is below 5.02, and from

$$m_h = 1.46\ \log C_5 - 1.2 \tag{4}$$

if the true magnitude is above 5.02. Ignorant of the true magnitude, a best estimate is found by taking the average of Eqs. (3) and (4).We have shown that this predicts the true magnitude to within approximately one unit.

6. Conclusions

Wavelet coefficients of the seismogram can be determined extremely rapidly and efficiently by the fast

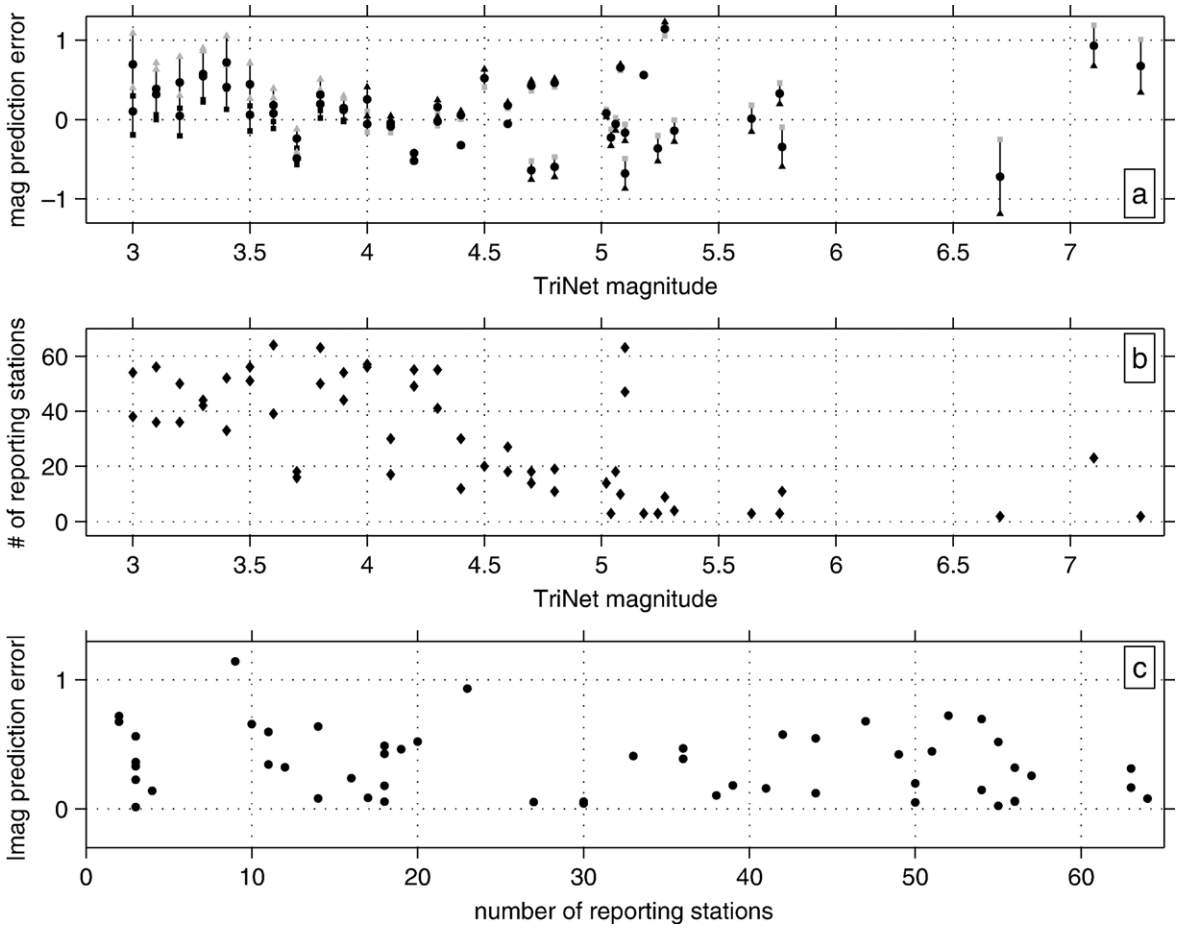

Fig. 6. Performance of the earthquake magnitude prediction algorithm. (a) Errors of the prediction from thresholded wavelet coefficients at scale 5, i.e. the horizontal distance of their average over all reporting stations to the regression lines in the bottom right panel of Fig. 5. Errors using the low-magnitude regression relation are shown as squares, those using the high-magnitude regression as triangles. They are connected by vertical lines and their averages are the black circles. When the regression line used is not appropriate for the true (TriNet) magnitude the squares or triangles are infilled gray. (b) Number of reporting stations as a function of TriNet magnitude of the events whose magnitude prediction errors are shown in (a). (c) Absolute values of the magnitude errors of the average of the high and low-magnitude regression predictions, i.e. the circles shown in (a), in function of the number of reporting stations.

lifting wavelet transform. Extracting amplitudes at individual scales is a very simple procedure, involving a mere handful of lines of computer code. Scale-dependent thresholded amplitudes derived from the wavelet transform of the first 3–4 s of an incoming seismic *P* arrival are predictive of earthquake magnitude, with errors of one magnitude unit for seismograms recorded up to 150 km away from the earthquake source.

Our procedure is a simple yet extremely efficient tool for implementation on low-power recording stations. It provides an accurate and precise method of autonomously detecting the incoming *P* wave and predicting the magnitude of the source from the scale-dependent character of its amplitude well before the arrival of damaging ground motion. Provided a dense array of networked seismometers exists, our procedure should become the tool of choice for earthquake early-warning systems worldwide.

Acknowledgments

We thank two anonymous reviewers for their comments on the submitted manuscript. This research was supported by a NERC Young Investigators' Award (NE/D521449/1) and a Nuffield Foundation grant for Newly Appointed Lecturers (NAL/01087/G) to FJS. Research leading to this publication was performed by BDED as part of his undergraduate M. Sci. project.

Appendix A

A simple algorithm for the forward CDF (2,4) biorthogonal wavelet transform, over five scales, of a signal whose length is a power of two. Based on the lifting scheme [22,24], we have optimized it for simplicity of implementation on a wide variety of platforms, rather than for memory or computational efficiency. No boundary effects of the finite-length input signals are taken into account. In a few lines of code, the input signal x is transformed into a same-length output x containing a Mallat multi-resolution ordering of scaling and wavelet coefficients:

```
lx=length(x);
for j=1:5;
  for n=2:2:lx-2
    x(n)=x(n)-[x(n-1)+x(n+1)]/2; end
  for n=5:2:lx-3
    x(n)=x(n)...
        -3*[x(n-3)+x(n+3)]/64...
        +19*[x(n-1)+x(n+1)]/64; end
x=[x(1:2:lx)*sqrt(2);...
  x(2:2:lx)/sqrt(2); x(lx+1:end)];
lx=length(x)/2^j; end
```

The inverse algorithm guarantees perfect reconstruction of the input signal from its CDF (2,4) wavelet transform obtained by the algorithm above:

```
for j=5:-1:1
  lx=length(x)/2^j;
  x(1:lx)=x(1:lx)/sqrt(2);
  x(lx+1:lx*2)=x(lx+1:lx*2)*sqrt(2);
  for n=3:lx-1
    x(n)=x(n)+3*[x(lx+n-2)...
        +x(lx+n+1)]/64...
        -19*[x(lx+n-1)...
        +x(lx+n)]/64; end
for n=1:lx-1
  x(lx+n)=x(lx+n)...
        +[x(n)+x(n+1)]/2; end
  y0=x(1:lx); y1=x(lx+1:lx*2);
  x(1:2:lx*2)=y0;x(2:2:lx*2)=y1;end
```

References

[1] H. Kanamori, Real-time seismology and earthquake damage mitigation, Annu. Rev. Earth Planet Sci. 33 (2005) 195–214, doi:10.1146/annurev.earth.33.092203.122626.

[2] R.M. Allen, H. Kanamori, The potential for earthquake early warning in southern California, Science 300 (2003) 786–789, doi:10.1126/science.1080912.

[3] Y.-M. Wu, H.-Y. Yen, L. Zhao, B.-S. Huang, W.-T. Liang, Magnitude determination using initial *P*-waves: a single-station approach, Geophys. Res. Lett. 33 (2006) L05306, doi:10.1029/2005GL025395.

[4] E.L. Olson, R.M. Allen, The deterministic nature of earthquake rupture, Nature 438 (2005) 212–214, doi:10.1038/nature04214.

[5] K. Aki, Scaling law of seismic spectrum, J. Geophys. Res. 72 (4) (1967) 1217–1231.

[6] H. Kanamori, D.L. Anderson, Theoretical basis of some empirical relations in seismology, Bull. Seismol. Soc. Am. 65 (5) (1975) 1073–1095.

[7] R. Abercrombie, The start of something big? Nature 438 (2005) 171–173.

[8] A.B. Lockman, R.M. Allen, Single-station earthquake characterization for early warning, Bull. Seismol. Soc. Am. 95 (6) (2005) 2029–2039, doi:10.1785/0120040241.

[9] B.L.N. Kennett, E.R. Engdahl, Travel times for global earthquake location and phase identification, Geophys. J. Int. 105 (1991) 429–465.

[10] A.E. Barnes, The calculation of instantaneous frequency and instantaneous bandwidth, Geophysics 57 (11) (1992) 1520–1524.

[11] I. Daubechies, The wavelet transform, time-frequency localization and signal analysis, IEEE Trans. Inf. Theory 36 (5) (1990) 961–1005.

[12] S. Mallat, A Wavelet Tour of Signal Processing, Academic Press, San Diego, Calif., 1998.

[13] P.D. Welch, The use of Fast Fourier Transform for the estimation of power spectra: a method based on time averaging over short, modified periodograms, IEEE Trans. Audio Electroacoust. 15 (1967) 70–73.

[14] J. Morlet, G. Arens, E. Fourgeau, D. Giard, Wave propagation and sampling theory. Part I: Complex signal and scattering in multilayered media, Geophysics 47 (2) (1982) 203–221.

[15] J. Morlet, G. Arens, E. Fourgeau, D. Giard, Wave propagation and sampling theory. Part II: Sampling theory and complex waves, Geophysics 47 (2) (1982) 222–236.

[16] B.B. Hubbard, The World According to Wavelets: the Story of a Mathematical Technique in the Making, 2nd Edition, A.K. Peters, Wellesley, Mass, 1998.

[17] O. Rioul, M. Vetterli, Wavelets and signal processing, IEEE Signal Process. Mag. 8 (4) (1991) 14–38.

[18] W. Sweldens, P. Schröder, Building your own wavelets at home, Wavelets in Computer Graphics, ACM SIGGRAPH Course notes, 1996, pp. 15–87.

[19] M. Vetterli, Wavelets, approximation, and compression, IEEE Signal Process. Mag. 18 (5) (2001) 59–73. doi:10.1109/79.952805.

[20] P. Kumar, E. Foufoula-Georgiou, Wavelet analysis for geophysical applications, Rev. Geophys. 35 (4) (1997) 385–412.

[21] G. Strang, T. Nguyen, Wavelets and Filter Banks, 2nd Edition, Wellesley–Cambridge Press, Wellesley, Mass, 1997.

[22] A. Jensen, A. la Cour-Harbo, Ripples in Mathematics, Springer, Berlin, 2001.

[23] A. Cohen, I. Daubechies, J. Feauveau, Biorthogonal bases of compactly supported wavelets, Comm. Pure Appl. Math. 45 (1992) 485–560.

[24] W. Sweldens, The lifting scheme: a custom-design construction of biorthogonal wavelets, Appl. Comput. Harmon. Anal. 3 (2) (1996) 186–200.

[25] I. Daubechies, W. Sweldens, Factoring wavelet transforms into lifting steps, J. Fourier Anal. Appl. 4 (3) (1998) 247–269.

[26] R. Calderbank, I. Daubechies, W. Sweldens, B.-L. Yeo, Wavelet transforms that map integers to integers, Appl. Comput. Harmon. Anal. 5 (3) (1998) 332–369.
[27] F.J. Simons, G. Nolet, J.M. Babcock, R.E. Davis, J.A. Orcutt, A future for drifting seismic networks, Eos Trans. AGU 87 (31) (2006) 305, 307.
[28] E.L. Olson, R.M. Allen, Earth science: is earthquake rupture deterministic? (Reply), Nature 442 (2006) E6, doi:10.1038/nature04964.
[29] P. Rydelek, S. Horiuchi, Earth science: is earthquake rupture deterministic? Nature 442 (2006) E5–E6, doi:10.1038/nature04963.
[30] I.M. Johnstone, B.W. Silverman, Wavelet threshold estimators for data with correlated noise, J. R. Stat. Soc., Ser. B 59 (2) (1997) 319–351.
[31] D. Donoho, I.M. Johnstone, Ideal spatial adaptation by wavelet shrinkage, Biometrika 81 (3) (1994) 425–455.